International Journal of Applied Engineering Research ISSN 0973-4562 Volume 13, Number 6 (2018) pp. 4306-4313

Effect of Sn on Thermal Kinetics of the Recrystallization for $Mg_{17}Al_{12}$ Phase in Mg-Al-Sn Rapidly Solidified Alloy

Emad M. Ahmed[1, 2], Sultan E. Alomairy[1]

[1]*Department of Physics, Faculty of Science, Taif University, 21974 Taif, P.O. Box 888, Kingdom of Saudi Arabia.*
[2] *Department of Physics, National Research Center, 33 EL Bohouth St., Dokki, Giza 12622, Egypt.*
Corresponding author

Abstract

Mg based biomaterials of nominal compositions Mg-6Al and Mg-6Al-2Sn (*at.* %) were prepared in the conventional cast and rapidly solidified ribbons conditions using melt spun technique. Deferential scanning calorimetry measurements followed by kinetics analysis at non-isothermal condition were performed to investigate the effect of Sn addition on the thermal kinetics of the $Mg_{17}Al_{12}$ recrystallization response. Moreover, Rietveld analysis was applied on the XRD results to evaluate the microstructure characterizations. XRD analysis showed the presence of only α-Mg phase with XRD peaks shifted to higher angular positions and confirmed a preferred orientation in the crystallographic plane (002). Most of Al and/or Sn have gone into α-Mg to form a supersaturated solid solution. The average crystallites size and micro-strain% of α-Mg phase are in the range of 30 nm and 0.32 respectively. Besides, the unit cell volume of the α-Mg decreases by 0.45 pm^3. DSC analysis confirmed a clear improvement in the thermal stability of the Mg6Al2Sn (RS) against $Mg_{17}Al_{12}$ recrystallization; its peak temperature was shifted to higher temperature, and activation energy rised from 64 KJ $mole^{-1}$ (which is near to the activation energy of vacancies migration, 48 KJ $mole^{-1}$) to 150 KJ $mole^{-1}$ (which is near to the activation energy of the Mg self-diffusion, 134 KJ $mole^{-1}$), respectively. Moreover, the non-isothermal transformations have been evaluated, and the calculated growth exponent (n=1.5 in the average) indicated that the recrystallization mechanism of γ-$Mg_{17}Al_{12}$ or β-Mg_2Sn is regarded as "nucleation and growth" with growth in a restricted direction. This may be correlated to the preferred orientation of the microstructure confirmed by XRD analysis.

Finally, the obtained results and their analysis both confirmed the influence of Sn content on the structural and thermal properties of the Mg6Al (RS) based biomaterial.

INTRODUCTION

Non-equilibrium processes, such as rapid solidification (RS), mechanical alloying (MA), vapor phase condensation, or irradiation/ion-implantation have been widely used for producing amorphous, intermetallic, and nanocrystalline materials. RS involves cooling of metallic melts at rates greater than 10^4 K/s, resulting in significant microstructure and constitutional developments, such as grain refinement, reduced segregation effects, formation of supersaturated solid solutions, and metastable crystalline intermediate and amorphous phases [1-4]. These benefits have improved the performance of the RS alloys such as the mechanical properties and the corrosion resistance.

On an one side, Mg and its alloys are recently considered as natural biomaterials since the elemental Mg is one of the main elements in the human body and their mechanical properties are similar to the natural bone. Moreover, the High corrosion of Mg and its alloys renders them to be very promising biodegradable materials since they can be adapted for medical purposes and then dissolved as they become undesirable. However, the byproducts of the corrosion process of Mg in a body, such as H_2 bubbles, may delay healing at the surgical site [5]. To overcome this, the corrosion rate of Mg and Its alloys should be inhibited to enhance the bone growth and consequently control the formation of H_2. It became well known, that control corrosion can be done mainly by microstructure development via specific processing techniques or developing surface treatments and alloying additions [6]. On the other side, Mg and its alloys are also well considered as applicable alloy in automobile industries owing to their low densities [7-9] for reducing the weight of automobiles and improving the energy consumption. Aluminum is the most applied alloying element in Mg alloys, forming the most famous Mg alloys such as AZ91, AZ31, and AM50 technical alloys. The Mg-rich hexagonal close-packed (HCP) α-phase and a near-stoichiometric $Mg_{17}Al_{12}$ γ-phase are the main phases in Mg-Al alloys which determine the mechanical and corrosion properties. Besides, Sn is added to Mg alloys for further enhance their mechanical properties [10] via formation of the intermetallic Mg_2Sn phase of remarkably higher melting point (770 °C) than the $Mg_{17}Al_{12}$ phase (463 °C).

RS process, as a specific processing technique, is considered as one of the highly potential approaches to improve the mechanical properties and to get better corrosion resistance by means of increase of solid solubility of the alloying elements in addition to refinement and homogeneity of microstructure [11-16]. However, applications of nanocrystalline Mg based alloys obtained by RS are limited by their low thermal stabilities owing to the grain growth as temperature increase. Thermodynamically, the solute atoms obtained in Mg-Al alloys by RS cause grain boundary (GB) segregation, reducing the GB free energy, and inhibit finally the grain growth [17-19]. Thus, the aim of the present study is to evaluate the effect of Sn addition on the thermal stability of the Mg6Al2Sn RS biomaterial by means of determination the kinetics for the recrystallization response of $Mg_{17}Al_{12}$.

EXPERIMENTS

Material preparation

Binary and ternary Mg based alloys of nominal compositions Mg-6Al and Mg-6Al-2Sn (*at* %) were prepared from pure Mg, Al, and Sn metals of purities 99.8, 99.9 and 99.75 (wt. %) respectively. The desired portion of the pure metals were melting and homogenizing in electrical muffle furnace under argon at 750 °C for 2 h, then poured into a graphite mold to produce rods of 25mm in length and 4mm in diameter. Rapidly solidified long ribbons of 50 μm thickness and 2mm width were prepared using melt spun technique. A molten alloy, as a stream at 850 °C, is ejected by argon gas at a gauge pressure of 1 bar from a silica tube with a 0.4mm orifice diameter, on a copper disc of 15 cm diameter coated by chromium, rotating at about 3000 rpm. The prepared ribbons are fairly uniform with deviation of 0.05 % mm and 3 μm in width and thickness.

Material Characterization.

XRD patterns were obtained using a 1390 Philips diffractometer with filtered Cu $K\alpha$ radiation at 40 kV and 20 mA. The X-ray samples were performed from a short length stuck on a glass slide using Vaseline. The X'pert HighScor 2004 program with Rietveld X-ray diffraction analysis were used to refine the XRD experimental results as mentioned in some previous works [20,21]. The reliability of the refinement results was judge by the pattern R factor (R_p), the weighted pattern R factor (R_{wp}), and the "goodness of fit" (GOF = $(R_{wp}/R_{xp})^2$ [22]. Initial structure parameters of all phases used for Rietveld method in this study were from ICCD (Inorganic Crystal Structure Database) cards. The parameters that had been refined simultaneously include scale factors, zero point shift, lattice parameters, atomic sites occupancies, isotropic or anisotropic temperature factors, profile shape parameter, FWHM (full width at half maximum) parameters, asymmetry and preferred orientation parameters.

DSC measurements were performed by NETZCH DSC 204 f1 phoenix. Samples of about 4 ±0.1 mg mass were used for the experiments varied out at different heating rates from room temperature up to 500°C under N_2 at a flow rate of 50 ml/min.

RESULTS

XRD analysis

According to the ternary Mg–Al–Sn phase diagram, the microstructures of the investigated Mg–Al–Sn alloys at room temperature consists of (α-Mg), eutectic (α-Mg) + γ-$Mg_{17}Al_{12}$, eutectic (α-Mg) + β-Mg_2Sn, and second phases of β-Mg_2Sn and γ-$Mg_{17}Al_{12}$ [23]. Fig.1 shows XRD patterns of the Mg-6Al-xSn RS ribbons, x = 0, 2. Generally, XRD patterns exhibit significant broadening peaks of hexagonal close packed (hcp) α-Mg phase (Card No. 00-001-1141) [24]. This effect can be attributed to the grain refinement and internal strain accommodated in the microstructure [25]. The corresponding XRD lines of γ-$Mg_{17}Al_{12}$ and β-Mg_2Sn intermetallic phases are absent and the lattice constants of Mg (RS); a and c, are lowered comparing to the stander Mg, as shown in Table.1.

Table 1. Lattice parameters a and c (Å), lattice parameters ratio (c/a), unit cell volume v (Å^3), crystallite size t (nm) and lattice strain % (ϵ %) of RS ribbons.

Samples	Phase	a	c	c/a	v	*t*	ϵ%
Mg6Al (RS)	Mg	3.190	5.183	1.6244	45.71	34	**0.324**
Mg6Al2Sn (RS)	Mg	3.193	5.189	1.6253	45.80	29	**0.326**

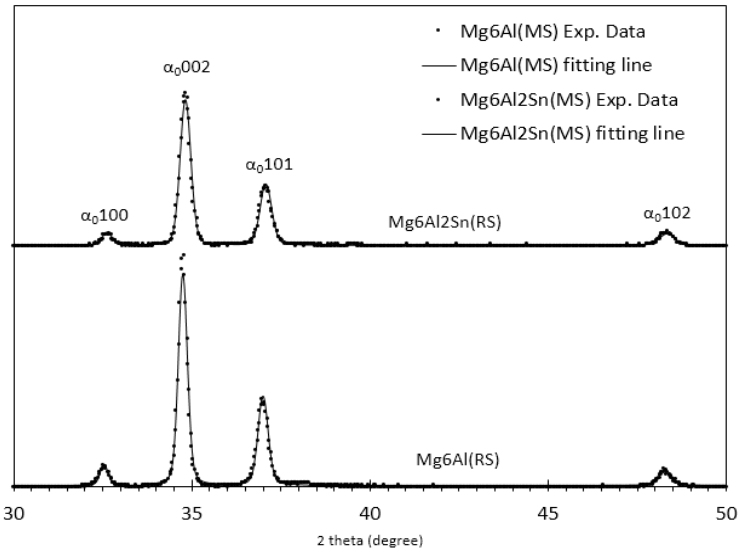

Figure 1. XRD patterns of Mg6Al (MS) and Mg6Al2Sn (MS) alloys (experimental data marked as points) and their Rietveld fitting (fitting data marked as lines).

This refers to the extension in the solid solubilities of the alloying elements in Mg (RS) phase and is related to the cooling rate obtained in the rapid solidification process, which was high enough to retain most of alloying elements in a supersaturated solid solution with Mg (RS) phase. Besides, during the rapid solidification process the eutectic transformations L→ α-Mg + γ-$Mg_{17}Al_{12}$, which happens in conventionally solidified Mg-Al alloy, are suppressed here to a great extent. Therefore, the XRD lines corresponding to the γ-$Mg_{17}Al_{12}$ phase were not observed. Moreover, average crystallites size and micro-strain% of Mg (RS) phase are calculated from the refined profile width parameters and summarized in Table 1. The calculated crystallites size and micro-strain% of Mg (RS) phase are of 29–34 nm and 0.315-0.326 ranges.

A preferred orientation-correction refinement for Mg (RS) phase had a great influence on the matching between the calculated and observed XRD lines intensities, and in turn on the Rietveld agreement factors for the melt spun ribbons. The crystallographic plane (1 0 1) of Mg has a much higher intensity than that of (0 0 2) in Mg6Al cast alloys. while, the Mg (RS) phase exhibited the crystallographic plane (002) as the highst one, owing to the spread of the molten alloy on the conducting substrate. This preferred orientation in RS Mg6Al and other RS materials have been reported earlier [26-28].

In addition, the high cooling rate obtained in rapid solidification had also a significant influence on the microstructure of the Mg (RS) phase as deduced by increasing of the lattice parameters ratio, *c/a* from the equilibrium value of 1.6236 up to 1.6244-1.6253 range as shown in Table.1. This means that the unit cell of the hexagonal Mg(RS) phase has been clearly deformed, owing to the rapid solidification. In case of Mg6Al (RS) alloy, the unit cell of the hexagonal Mg (RS) phase shrunk, via the substitutional dissolution of Al atoms in the Mg (RS) (the unit cell volume of the Mg(RS) decreases from the standard value of 46.17 down to 45.71 by decrease of 0.46 Å). This can be related to the variation of atomic radius of the constitute atoms from 160 nm (Mg atom) to 143 nm (Al atom). In case of Mg6Al2Sn (RS) alloy. No further decrease in the Mg unit cell volume could be observed, owing to that the atomic radii of Mg and Sn are much close [29], therefore any substitutional dissolution of Sn in Mg would not produce much change in the unit cell volume of the Mg(RS). In fact, the absence of XRD lines corresponding to the intermetallic phases does not mean that the alloying elements are dissolved completely in the main matrix. Refinement structure obtained during the rapid solidification for the RS ribbons makes it difficult to detect the nanostructured intermetallic phases with undetectable XRD peaks. This nanostructured intermetallic phases with little contents usually produce much broad and small peaks which disappeared with the background of the XRD pattern.

DSC analysis

Fig.2 represents the DSC results of Mg6Al and Mg6Al2Sn cast alloys, obtained during heating cycle form room temperature to 500 °C, at heating rate of 20 °C/min. DSC chart of Mg6Al cast alloy reveals an endothermic peak corresponding to melting of the $Mg_{17}Al_{12}$ phase around 443 °C. This endothermic peak is shifted to lower temperature of about 436 °C in case of Mg6Al2Sn cast alloy. In rapidly solidified ribbons, the high cooling rate obtained in the RS process by melt spun technique allows very short time for the solidification of base Mg and alloying elements. The alloying elements Al and Sn were not allowed to precipitate as new phases as usual in casting processes; they are trapped in the Mg matrix forming a supersaturated solid solution of Al and Sn in Mg. Therefore, it would be expected to observe exothermic peaks in of the DSC chart during the heating cycle for the rapidly solidified alloys. In addition, non-isothermal DSC analysis was used to investigate the recrystallization kinetics of precipitating phases as shown in Fig.3, No endothermic peaks are observed at the heating cycle of the DSC charts as expected. Instead, exothermic peaks are observed, which corresponding to a recrystallization process of the precipitated phases. As a result of the non-isothermal reaction between Mg and the alloying elements, an energy dissipated during the recrystallization process. The exothermic peak temperature of the recrystallization reaction corresponds to the point of maximum enthalpy associated with the highest rate of phase recrystallization. These exothermic peaks, observed in the rapidly solidified alloys, may originate from the grain growth, strain relaxation and decomposition of metastable solid solution into component elements and phase precipitation [30,31]. In case of the Mg6Al (RS) sample, the only exothermic peak observed is corresponding to the $Mg_{17}Al_{12}$ phase, while in case of Mg6Al2Sn (RS), there are two exothermic peaks corresponding to the γ-$Mg_{17}Al_{12}$ and β-Mg_2Sn precipitations as shown in Fig.3. The typical heat flow with temperature in the heating cycle for each exothermic peak are recalculated by subtraction the DSC ground signals as shown in Fig. 3(a), 4(a) and 5(a). It is clear that these exothermic peaks move toward higher temperatures as much as the heating rate increases, which suggests that the solid state reactions are thermally activated and kinetically controlled. In addition, at the same heating rate, it is obvious that the exothermic peak temperatures of the $Mg_{17}Al_{12}$ are shifted to higher temperatures in the Mg6Al2Sn (RS) comparing to Mg6Al (RS) ribbons.

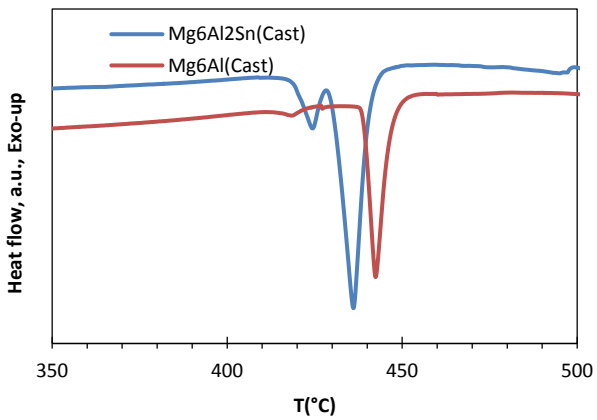

Figure 2. Heat flow versus temperature for Mg6Al and Mg6Al2Sn conventional cast alloys

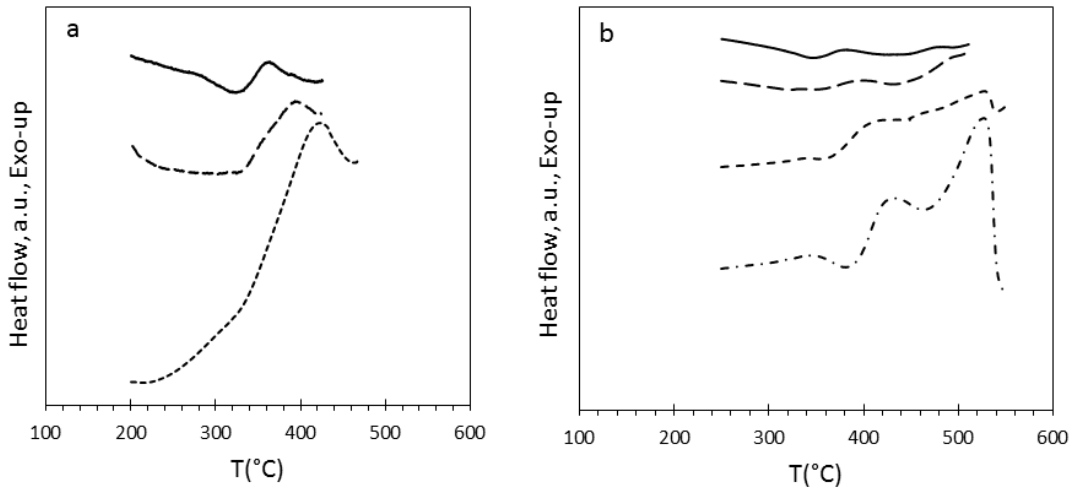

Figure 3. DSC signals with temperature for Mg6Al (RS) (a), and Mg6Al2Sn (RS) (b) at different heating rates (5, 10, 20, and 40 °C/min).

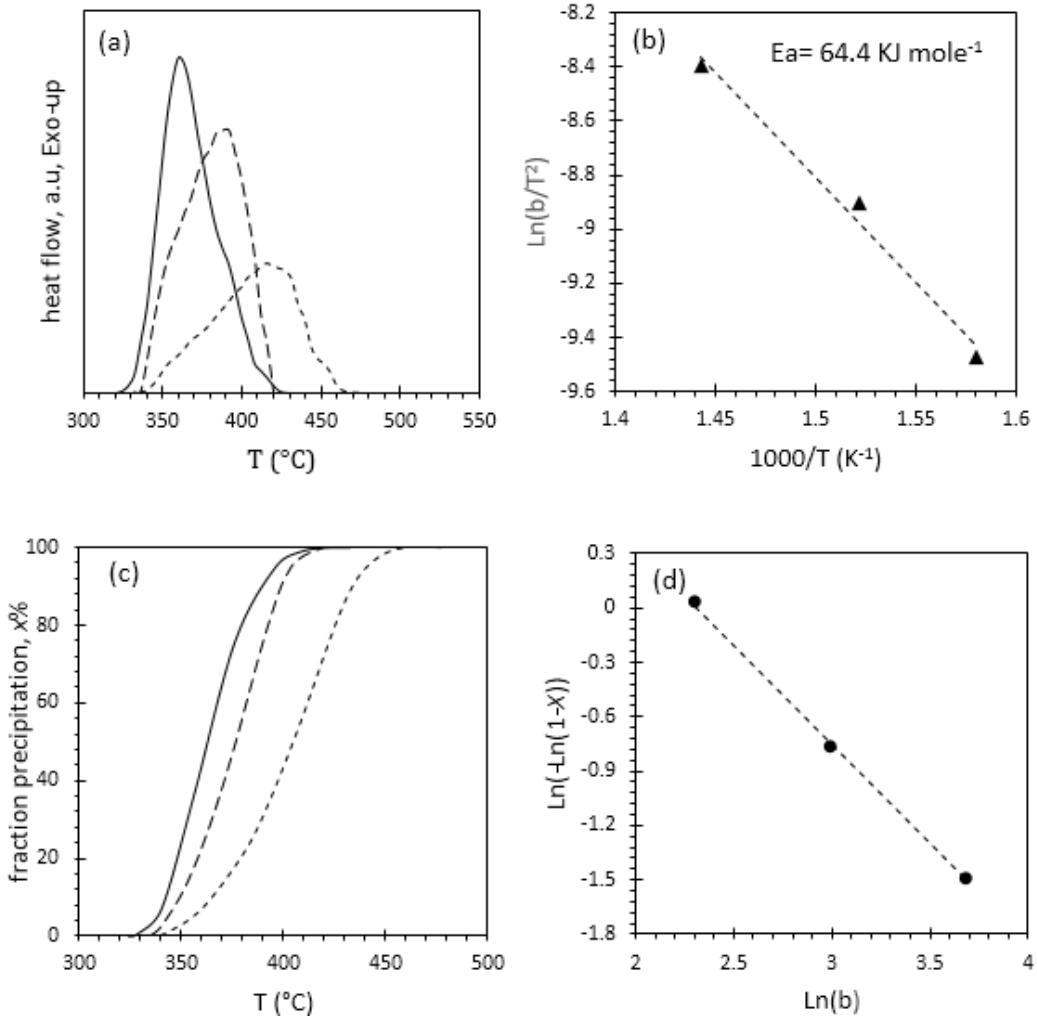

Figure 4. Typical DSC curves of $Mg_{17}Al_{12}$ phase in Mg6Al (MS) at heating rates of 10, 20, 40 °C/min (a), Kissinger analysis and activation energy calculation (b), fraction precipitation x % with temperature (c) and n calculation (d).

Activation Energy:

To follow the kinetics of these recrystallizing phases during the heating cycle of DSC measurements, John-Mehl-Avrami-Kilmogoroc (JMAK) relation was used, in which volume fraction of precipitate phases is related to kinetics laws of growth. Based on this relation, for non-isothermal processes, several methods have been developed [32-36] for calculation of kinetic parameter. One of them is the Kissinger method [34], which takes into account the peak positions' shift under various heating rates. The relation between peak temperature T_p and heating rate b can be written as the following:

$$\ln\left(\frac{b}{T_p^2}\right) = -\frac{E_a}{RT_P} + C \quad (1)$$

Where, E_a: the activation energy (J mole^{-1}), R the universal gas constant (8.314 J/mole K), C is a constant. Figs 3, 4, and 5(b) represent the evolution of ln (b/T_p^2) versus (1000/T_p) of the different recrystallizing phases. It is so simply to calculate the slope of these curves to determine the activation energies as reported in Table 2. The calculated activation energies of $Mg_{17}Al_{12}$ recrystallizations in Mg6Al (RS) and Mg6Al2Sn (RS) alloys are 64.4 KJmole^{-1}, which consistent with the results reported recently [37], and 154 KJmole^{-1}, respectively. This indicates that the addition of 2 *at*% Sn caused an enhancement of the activation energy and results in an improvement in the thermal stability of the Mg6Al2Sn (RS) against $Mg_{17}Al_{12}$ recrystallization. This is consistent with what was recently reported [38], that an addition of 2 wt. % Sn to AZ80 (after homogenization at 450 °C for 12h) have retarded the dynamic recrystallization of the $Mg_{17}Al_{12}$ phase during hot press at 350 °C for AZT802 comparing to the AZ80, leading to less contents of the $Mg_{17}Al_{12}$. Sn element appears to impose resistance to the crystallization of the major $Mg_{17}Al_{12}$ phase, possibly by blocking the path of Mg and Al diffusion.

The activation energy for the starting recrystallization of $Mg_{17}Al_{12}$ (in case of Mg6Al2Sn (RS)) was acquired to be 154 kJ/mole, which is close to the self-diffusion activation energy in magnesium (134 KJmole^{-1})[39] and higher than that for vacancy migration (48 KJmole^{-1} [40]). This means that, quenched-in vacancies, formed during rapid solidification process, which was effective for this precipitation (in case of Mg6Al (RS) since its activation energy of 64 KJmole^{-1} was near to that for vacancy migration of 48 KJmole^{-1}), are no longer effective in this type of precipitation with existence with Sn content. Besides, the activation energy of Mg_2Sn recrystallization for Mg-6Al-2Sn (RS) is obtained as high as 384 KJmole^{-1}. This value is found to be higher than the activation energy of formation for the same phase reported in mixture of Mg-5Sn (281.7 KJmole^{-1}) [41]. This can be attributed to the high dislocation concentration obtained in the rapid solidification process, which may hinder the precipitation process and enhancing the activation energy required for starting phase precipitation.

Evolution of the non-isothermal transformation

Based on the DSC data of the exothermic peaks, the transformed fractions of $Mg_{17}Al_{12}$ and Mg_2Sn phases as a function of scan temperature for different heating rates are plotted in Fig. 3, 4 and 5(C). The transformed fraction, x, measures the extent of a specific precipitation reaction at a given scan temperature and is given by [42].

$$x = \frac{Ap}{Af} \quad (2)$$

where A_p is the partial area of the relevant peak between the onset temperature and the temperature at which the transformed fraction is being calculated and A_f is the total area of the peak between the onset and ending temperatures. The x-T curves obtained are sigmoidal in shape (S-shaped), showing that for a fixed heating rate, the transformed fraction increases as the temperature increases. However, for a given temperature, the transformed fraction decreases as the heating rate increases. These features are explained by the effects of temperature and time on the diffusion of solute atoms. Increasing the temperature increases the diffusion and consequently the transformed fraction. On the contrary, increasing the heating rate gives insufficient time for solute atoms to diffuse, thereby decreasing the transformed fraction.

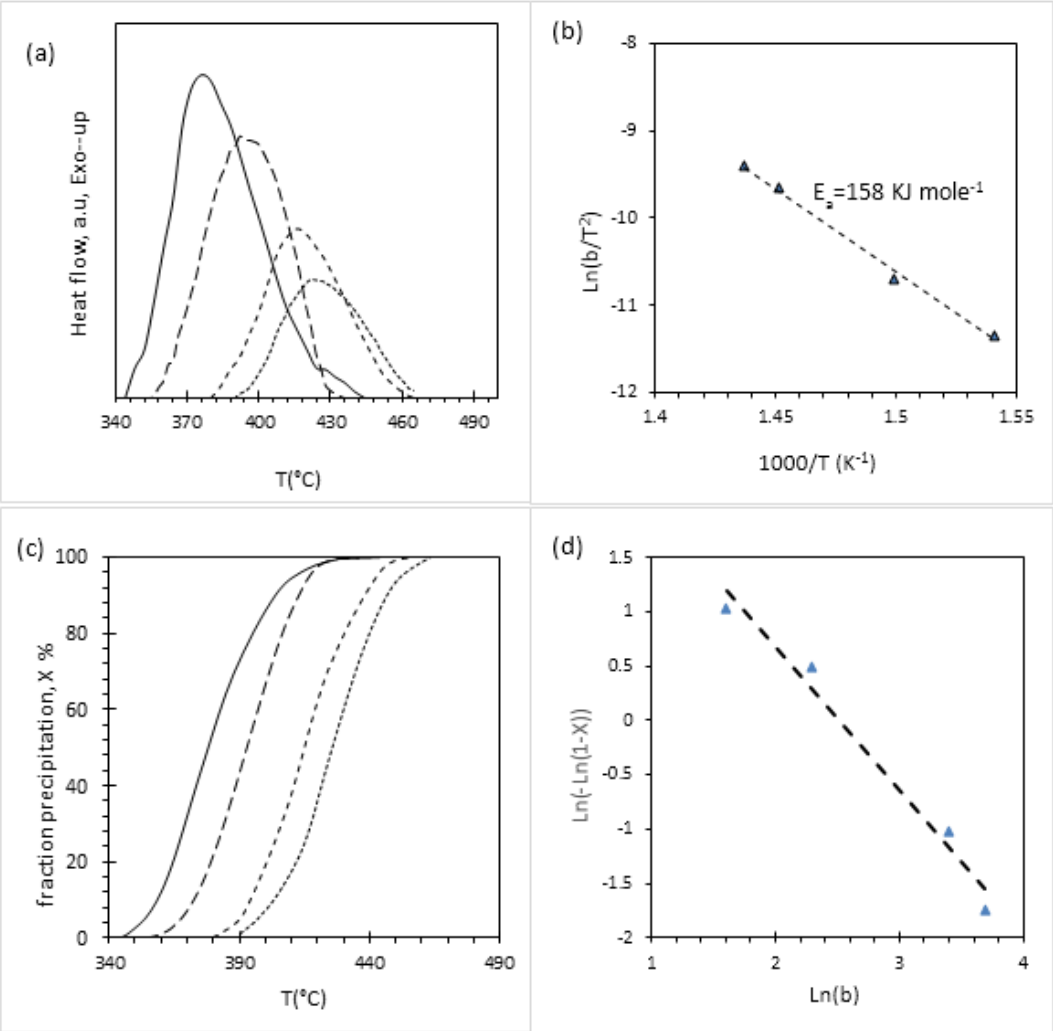

Figure 5. Typical DSC curves of $Mg_{17}Al_{12}$ phase in Mg6Al2Sn (RS) at heating rates of 5, 10, 30, and 40 °C/min (a), Kissinger analysis and activation energy calculation (b), fraction precipitation *x* % with temperature (c) and *n* calculation (d).

Growth exponent

The growth exponent, *n* (also referred to as Avrami exponent), is used in the analysis of the kinetics of solid state phase transformations to describe the transformation mechanism and growth morphology [43, 44]. It can be calculated for non-isothermal transformations using the following equation [45, 46]:

$$n = \frac{\ln(-\ln(1-x))}{\ln(b)} \quad (3)$$

where *x* is the fraction precipitated at a given temperature *T* for the heating rate *b*. For any fixed temperature *T*, the values of *x* at different heating rates can be determined, from the *x*-*T* curves shown in Fig. 4(c), 5(c), and 6(c), then recalculated for drawing the plot of $\ln(-\ln(1-x))$ vs $\ln(b)$. According to Eq. (3), the resulting plot yields a straight line with slope *n*, which is the growth exponent at certain temperature *T*. In both Mg6Al (RS) and Mg6Al2Sn (RS), the average calculated growth exponent for the formation of $Mg_{17}Al_{12}$ and Mg_2Sn were about 1.5 with which it is confirmed that the recrystallization mechanism of $Mg_{17}Al_{12}$ and Mg_2Sn is regarded as "nucleation and growth". The value of *n* less than 2 refers to a restricted growth in a particular direction, instead of the growth in 3 direction for *n* = 3 or 4. This is consistence with the results obtained by XRD analysis since the XRD pattern showed a preferred orientation in the crystallographic plane (002) through which the diffusion of solute atoms may be limited.

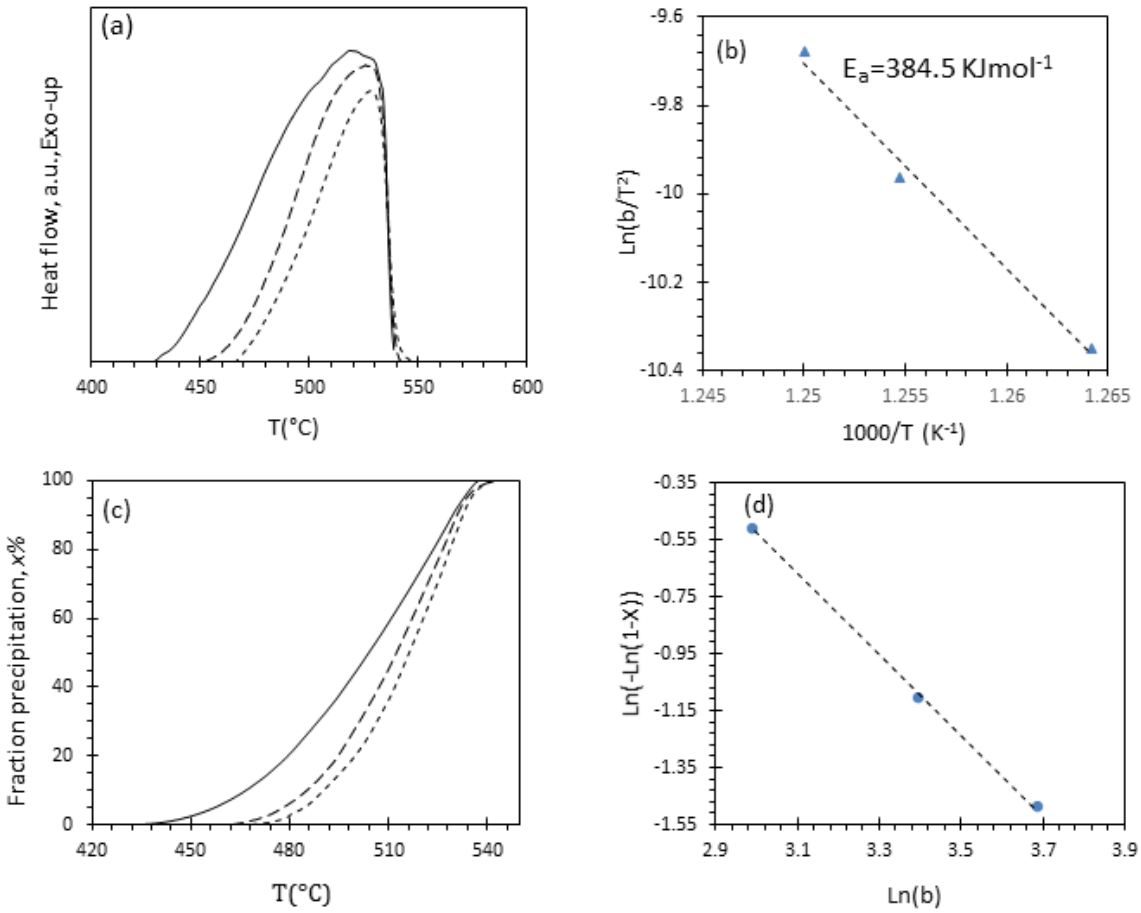

Figure 6. Typical heat flow signals of Mg_2Sn precipitations at heating rates of 20, 30 and 40 °C/min (a), Kissinger analysis and activation energy calculation (b), fraction precipitations of Mg_2Sn with temperature (c) and Avrami parameter calculation.

CONCLUSIONS

Mg-6Al and Mg-6Al-2Sn alloys have been prepared via conventional cast and rapid solidification using melt spun technique. XRD results confirmed the absence of any XRD lines corresponding to any intermetallic phases, only broadening XRD peaks of α-Mg observed at angular positions shifted to higher values referring to the formation of supersaturated solid solution of Al and Sn in Mg. Rietveld analysis has been performed successfully and the microstructure parameters have been estimated. The crystallite size of the Mg main matrix lowered to around 30 nm, while micro-strain% raised to 0.32. The unite cell moreover, deformed by means of the decrease of both lattice parameters and the unite cell volume by 0.46 Å^3, owing to the dissolution of Al in Mg. As a result of the spread of the molten alloys on the conducting substrate during the rapid solidification via melt spun technique, a preferred orientation of has been observed at the crystallographic plane (002) of Mg. The effect of Sn alloying on the recrystallization kinetics of $Mg_{17}Al_{12}$ has been studied using DSC analysis followed by kinetics analysis at non-isothermal condition. The exothermic peak corresponding to the recrystallization of $Mg_{17}Al_{12}$ with peak temperature shifted to higher value and the activation energy required for initiation the recrystallization process raised from 64 to 154 KJ mole^{-1}. This indicated that the precipitation of solute atoms (Al or Sn) via vacancies migrations, in Mg6Al (RS) was replaced by the Mg self-diffusion process in after adding 2 % Sn. The evaluation of the non-isothermal transformations of $Mg_{17}Al_{12}$ enabled us to determine the growth exponent (n=1.5 in the average), which indicated that the recrystallization mechanism of γ-$Mg_{17}Al_{12}$ or β-Mg_2Sn is regarded as "nucleation and growth" with growth in a restricted direction. The obtained results and their analysis both confirmed the influence of Sn content on the structural and thermal properties of the Mg6Al (RS) based biomaterial.

ACKNOWLEDGEMENTS:

Authors would like to thanks Taif University for finance support for this work through scientific contact (1-438-5847).

REFERENCES

[1] C. SURYANARAYANA, *Non-equilibrium Processing of Materials,* 1st ed, (Pergamon, 1999).

[2] S . K. DAS, *Reviews in Particulate Materials*,Vol. 1 (Metal Powder Industries Federation, Princeton, NJ, 1993).

[3] H. H. LIEBERMANN, *Rapidly Solidified Alloys: Processes, Structures, Properties, Applications*, (Marcel Dekker, New York, NY, 1993).

[4] T. R. ANANTHARAMAN and C. SURYANARAYANA, Rapidly Solidified Alloys: A Technological Overview" (Trans Tech Publications, Aedermannsdorf, Switzerland, 1987).

[5] A. Meyer-Lindenberg, H. Windhugen and F. Witte: US 200410241036, 2006.

[6] H. Hornberger, S. Virtanen and A. R. Boccaccini, Acta Biomater. **8**, 2442 (2012),.

[7] H. Pan, Y. Ren, H. Fu, H. Zhao, L. Wang, X. Meng, G. Qin, J. Alloys Compd. **663**, 321 (2016) .

[8] C.J. Bettles, M.A. Gibson, JOM **57**, 46 (2005).

[9] F.S. Pan, M.B. Yang, D.F. Zhang, L.Y. Wang, P.D. Ding, Mater. Sci. Forum **413418**, 488 (2005).

[10] H. Ren, W. Hu, D. Li, X. Zeng, X. Yang, X. Zeng, X. Yang, B. Huang, Y. Liu, J. Magnes. Alloy **4,** 62 (2016) .

[11] J . D. COTTON, J. Electrochem. Soc. **136,** 523 (1989).

[12] F . HEHMAN, F . SOMMER, H. JONES and R. G. J . EDYVEAN, J. Mater. Sci. **24,** 2369 (1989).

[13] C. B. BALIGA, P . TSAKIROPOULOS and C. JEYNES, *ibid.* **26,** 1497 (1991).

[14] C. B. BALIGA and P . TSAKIROPOULOS, *Mater. Sci.&Eng.* **A134,** 1029 (1991).

[15] G. L. MAKAR, J . KRUGER and K. SIERADZKI, J. Electrochem. *Soc.* **139,** 47 (1992).

[16] G. L Makar, J. Kruger, K. Sieradzki, Corrosion Sci. **34**(8)**,** 1311 (1993).

[17] T. Chookajorn, H.A. Murdoch, C.A. Schuh, Science **337**, 951 (2012) .

[18] K.A. Darling, M.A. Tschopp, B.K. VanLeeuwen, M.A. Atwater, Z.K. Liu, Comput. Mater. Sci. **84**, 255 (2014) .

[19] K.A. Darling, B.K. VanLeeuwen, J.E. Semones, C.C. Koch, R.O. Scattergood, L.J. Kecskes, S.N. Mathaudhu, Mater. Sci. Eng. **A 528**, 4365 (2011).

[20] M. A. Amin , S. A. Fadlallah , G. S. Alosaimi , E. M. Ahmed , N.Y Mostafa, P. Roussel , S. Szunerits , R. Boukherroub, ACS Appl Mater Interfaces. **9(35)** 30115 (2017).

[21] M. A. Amin, E. M. Ahmed, N. Y. Mostafa, M. M. Alotibi, G. Darabdhara, M. R. Das, J. Wysocka, J. Ryl, S. S. Abd El-Rehim, *ACS Appl. Mater. Interfaces* **8 (36),** 23655 (2016).

[22] R.A. Young, The Rietveld Method, in Introduction to the Rietveld Method, edited by R.A. Young (Oxford University Press, New York, 1996).

[23] E. Doernberg, A. Kozlov, R. Schmid-Fetzer, ASM Int. **28,** 523 (2007).

[24] Hanawalt. et al., *Anal. Chem.*, **10**, 475(1938).

[25] J. Cai, G. C. Ma, Z. Liu, H. F. Zhang, Z. Q. Hu., J Alloys Compd **422**, 92(2006).

[26] H. Jones, "Rapid Solidification of Metals and Alloys" (Institution of Metallurgists, London, UK, 1982).

[27] E. Laine, I . L Ahteenm, AKI , *J. Mater. Sci.* **6** (1971) 1418.

[28] S. S. CHO, B. S. CHUN, C. W. WON, S. D. KIM, B. S. LEE, H. BAEK, J. Mater. SCI. **34** 4311 (1999).

[29] N. N. Greenwood, A. Earnshaw, *Chemistry of the Elements*, 2nd ed, (Butterworth-Heinemann).

[30] Q. ZENG, I. BAKER, V. MCCREARY, Z. YAN, J. Mag. Mag. Mater. **318** (1−2), 28 (2007).

[31] Z. LUO, Z. Q. LI. Mater. Sci. Eng. A **459** (1−2), 47 (2007).

[32] F.L. Cumbrera, F. Sanchez-Bajo, Thermochim. Acta **266,** 315 (1995).

[33] T. Kemeny, J. Sestak, Thermochim. Acta **110**, 113 (1987).

[34] H. Kissinger, Anal. Chem. **29**, 1702 (1957).

[35] A. Munoz, F.L. Cumbrera, Thermochim. Acta **144**, 123 (1989).

[36] J. Malek, Thermochim. Acta **147**, 377 (1989).

[37] F. Sahnoune, M. FatmiḊ, H. Belhouchet, M. Heraiz and N. Saheb, , International Journal of Advance Industrial Engineering, **1**(3) (2013)

[38] L. Jiang, W. Huang, D. Zhang, F.Guo, H. Xue ,J. Xu, F. Pan, J. Alloys Comp. **727**, 205 (2017).

[39] G. Neumann, C. Tuijn, *Self-diffusion and Impurity Diffusion in Pure Metals: Handbook of Experimental Data*[M], 1st ed, (Elsevier, 2011.)

[40] T.J. Pike, B. Noble, Journal of Less Common Metals, **30**, 63 (1973).

[41] W. U. Yu-feng, D. U. Wen-bo, Z. U. O. Tie-yong, Trans. Nonferrous Met. Soc. China **19**, 1196 (2009).

[42] K.S. Ghosh, N. Gao, Trans. Nonferrous Met. Soc. China **21,** 1199 (2011).

[43] I. Sinha, R.K. Mandal, J. Non-Cryst. Solids **357**, 919 (2011).

[44] J. Wang, H.C. Kou, X.F. Gu, J.S. Li, L.Q. Xing, R. Hu, L. Zhou, Mater. Lett. **63,** 1153 (2009.

[45] J. Farjas, P. Roura, Acta Mater. **54**, 5573 (2006).

[46] F. Liu, F. Sommer, E. J. Mittemeijer, J. Mater. Sci. **42,** 573 (2007).